CFD Analysis on the Dynamic Behaviour of Pivot Point for a KCS During Ship Turning Manoeuvre in Waves

Jongyoon Kim[1], Seungcheol Kwon[2], Minkyu Kim[3], Jiung Choi[3], Jong-youp Baek[4], Gil-young Kong[1], Soonseok Song[5,*] and Daejeong Kim[1,*]

[1]Division of Navigation Convergence Studies, Korea Maritime & Ocean University, South Korea

[2]Korea Institute of Maritime and Fisheries Technology, 367, Haeyang-ro, Yeongdo-gu, Busan, Republic of Krea

[3]Busan Harbor Pilot Association, Busan, Republic of Korea

[4]Nippon Kaiji Kyokai, Busan, Republic of Korea

[5]Department of Naval Architecture and Ocean Engineering, Inha University, 100, Inha-ro, Michuhol-gu, Incheon, Republic of Korea

Abstract: A comprehensive grasp of vessel manoeuvring characteristics is indispensable for ensuring precise handling and maritime safety. In practice, for Masters and Pilots, an intuitive understanding of the ship's rotational centre—the pivot point—is often more critical than merely fulfilling performance metrics. This study systematically investigated the dynamic migration of the pivot point for a KCS vessel under various wave conditions (initial direction, length, and height), addressing a topic relatively overlooked in conventional manoeuvring studies. The research methodology employed a high-fidelity URANS approach combined with a dynamic overset grid method to simulate 6-DOF turning circle manoeuvres. Through numerical analysis, stable pivot point behaviour under general sea conditions was confirmed, while non-linear and abrupt positional shifts under critical threshold conditions were quantitatively identified. Notably, the results numerically demonstrated that the pivot point migrated sharply beyond the bow boundary under extreme wave heights or when encountering short waves in quartering sea. This finding confirms that the pivot point is dynamically repositioned by changes in hydrodynamic moments driven by sway and yaw motions. These findings serve as a practical reference for operators to pre-emptively recognize and respond to changes in rudder effectiveness and turning moments when manoeuvring in adverse weather conditions.

Keywords: Pivot point, Dynamic behaviour, Manoeuvrability in waves, Computational Fluid Dynamics, Time-series analysis, Operational perspective, KCS.

1. INTRODUCTION

A comprehensive grasp of vessel manoeuvring characteristics is indispensable for ensuring precise handling and maritime safety. In particular, the increasing size of vessels demands more precise control to ensure safety in a real seaway. Recent investigations indicate that over 75% of marine accidents are attributed to human error [1]. Notably, these casualties, including collisions and groundings, frequently stem from a lack of understanding regarding complex ship manoeuvring behaviours, such as the hydrodynamic interactions among the hull, propeller, and rudder, the impact of external disturbances, and shallow water effects. This comprehensive understanding is particularly critical in confined harbour waters where manoeuvrability is restricted, making it imperative for Masters and Pilots to accurately predict ship motions to ensure safe berthing and unberthing operations. To mitigate such errors, autonomous navigation is emerging as a future solution [2]. Yet, whether a vessel is manually operated by Masters today or controlled by algorithms in the upcoming autonomous era, the fundamental physics of ship manoeuvring remain unchanged. Thus, accurately analysing these dynamic manoeuvring characteristics is an indispensable task for preventing human errors in existing vessels.

Discussion around ship manoeuvring performance has long been a subject of interest; however, until now the focus has been on satisfying quantitative criteria as tactical diameter and advance, rather than investigating it from an operational perspective [3-7]. In reality, the primary concern for captain and pilot is not the mere fulfilment of performance metrics, but the intuitive understanding of the ship’s rotational centre, namely the pivot point. This is because vessel control strategies must be fundamentally determined depending on the location of the pivot point [8]. Despite its practical significance, research on the dynamic migration of the pivot point remains limited. Thus, more extensive investigations of the pivot point position in real sea states are essential for operators to ensure safe manoeuvring.

In actual sea conditions, ships under manoeuvring are affected by various environmental disturbances

---

*Address correspondence to this author at the Division of Navigation Convergence Studies, Korea Maritime & Ocean University, South Korea; E-mail: s.song@inha.ac.kr; kdj4907@kmou.ac.kr

Received on 05-03-2026 Accepted on 13-04-2026 Published on 17-04-2026

E-ISSN: 2409-9848/26

such as waves, currents, and wind, which result in marked differences in their manoeuvring performance. Especially, the location of the pivot point is not a constant value but fluctuates in response to these environmental loads. Among these external forces, waves have been recognised as the most significant factor that leads to substantial discrepancies in the pivot point location. Therefore, it is important to incorporate wave variables for an accurate investigation into the dynamic migration of the pivot point. Manoeuvring in waves has been addressed by an International Towing Tank Conference Specialist Committee [9] and has also been discussed at MARSIM conferences [10]. While previous studies have made meaningful contributions to identifying the time-series migration of the pivot point, their scope has been largely limited to calm water conditions. Subsequent research introduced numerical methods combining potential and viscous flow calculations, thereby overcoming the limitations of conventional analytic solutions [11]. This approach enabled more precise analysis of the time-series behaviour of the pivot point within calm water conditions. In addition, A study has also quantitatively presented the positional changes of the pivot point over time during astern manoeuvring through verification experiments [12]. The scope of research has further expanded to analysing the dynamic migration of the pivot point as perceived by operators, utilizing ship handling simulation that approximate port manoeuvring environments [13]. However, the systematic consideration of wave conditions, which significantly affect manoeuvring performance in actual sea areas, remains notably absent. This is likely attributable to the practical difficulties in experimentally acquiring the ‘instantaneous’ and ‘dynamic’ kinematic data necessary to derive the pivot point under wave conditions. Additionally, the substantial modelling complexity and computational cost associated with reproducing wave-induced nonlinear hydrodynamic forces through numerical methods pose further challenges [14].

Meanwhile, with the significant advancement in computational power, Computational Fluid Dynamics (CFD) has enabled detailed hydrodynamic analyses of ship manoeuvrability. This approach can precisely estimate the effects of the complex interaction between the hull and other structural components such as the rudder and propeller. Moreover, it is worth mentioning that this method can provide more reliable ‘instantaneous’ and ‘dynamic’ manoeuvrability data than conventional methods by incorporating viscous and rotational effects in waves. CFD approach can make results remarkably consistent with experimental data in calm water by directly accounting for actual rudder movements and propeller rotations [15]. Furthermore, the dynamic overset grid method maintains good agreement with experimental results even when relatively coarse unstructured grids are employed, thereby effectively reducing computational costs [16].

Following the validation of high similarity to experimental results and practical efficiency in calm water, the application of the dynamic overset grid method has been extended to simulate complex manoeuvres in waves. This approach enables the reproduction of course-keeping and zigzag tests while fully incorporating the ship’s 6-degrees-of-freedom (6-DOF) motions across different wave directions [17, 18]. In addition, the capability to resolve variations in manoeuvring performance has been verified through simulations of course keeping and turning circle tests conducted on the standard KCS model under various wave directions, including following waves [3-5].

To the best of our knowledge, there exists no specific study investigating the effects of waves on the dynamic migration of the pivot point. Therefore, the aim of this study is to quantitatively analyse the variations in the pivot point position based on time-series data obtained from CFD simulations of turning manoeuvres under both calm water and various wave conditions. Through this analysis, we intend to provide practical insights into the variability of the pivot point that ship operators must consider during navigation in adverse weather conditions.

2. METHODOLOGY

Figure **1** shows the research methodology followed in this work for the analysis of the pivot point position, based on kinematic data from direct CFD manoeuvring simulations. This methodology consisted of four major steps. The first step addressed the fundamental components of the ship model, enabling movement in six degrees of freedom (6-DOF) with a moving rudder and an actuator disk. Furthermore, the environmental conditions were defined, with wave characteristics serving as the primary independent variables of this study. Specifically, CFD simulations were carried out under various wave properties, such as initial wave direction, wavelength, and wave height. In the second step, numerical modelling was performed to simulate the integrated manoeuvring sequence. the dynamic overset grid method was adapted to the hull and rudder regions. To facilitate large amplitude motions in waves, surrounding overset grids for the hull region were employed. Additionally, the rudder overset grids enabled precise control of rudder movements during ship turning manoeuvres. The body force method was applied to implement an actuator disk instead of a discretized propeller. By utilizing a PID feedback controller to regulate rudder rotational speed, the ship

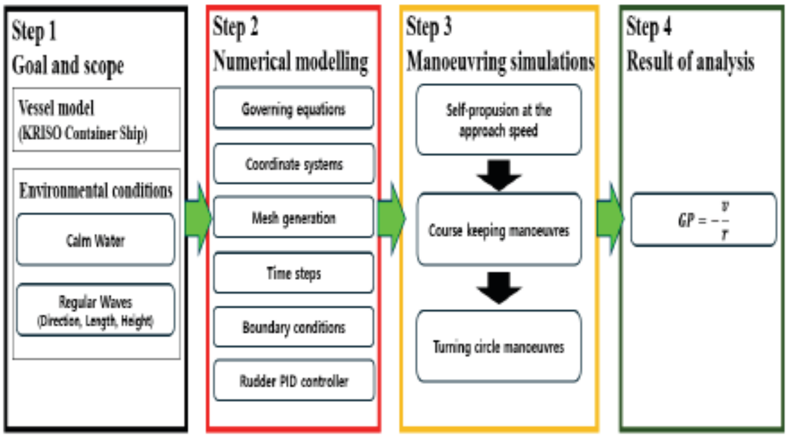

Figure 1: An overview of research methodology for analysis the pivot point position.

was able to maintain its course even under the influence of external disturbances. In the third step, the self-propulsion condition was established prior to the turning manoeuvre tests. Once the self-propulsion computations were completed, the rotational speed of the actuator disk was fixed. Subsequently, a course-keeping phase was initiated to stabilize the vessel's heading. After reaching a steady state, the turning manoeuvre was performed to extract the following time-series kinematic data: 1) v (m/s), the sway velocity, 2) r(rad/s), the yaw rate. Finally, the data obtained through these processes were substituted into the formula for determining the pivot point position.

2.1. Pivot Point

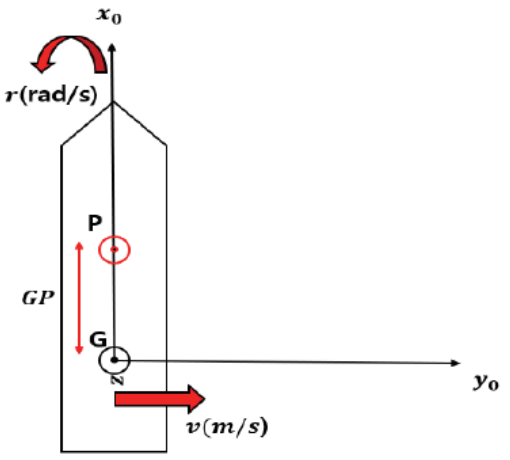

Figure 2: Geometric configuration of the pivot point and coordinate axes.

When a vessel undergoes a turning manoeuvre, a stationary point exists along the ship's longitudinal centreline that remains invariant to the dynamic changes in motion. This point is defined as the Pivot Point, the centre of the vessel's rotational motion [19]. In physical terms, the pivot point is the location where the lateral speed and the tangential speed induced by rotation exactly cancel each other, resulting in a zero net sway velocity. It is, therefore, characterized by a zero-drift angle [10]. It can be described as follows:

$$v + GP \cdot r = 0 \tag{1}$$

by rearranging Eq. (1), we obtain the expression for the pivot point as below:

$$GP = -v/r \tag{2}$$

where v is the sway velocity, r is the yaw rate and GP is the distance from the centre of gravity to the pivot point, where the positive x-direction points towards the bow.

2.2. Ship Geometry and Particulars

A KCS container ship model (with a scale factor of 75.24) combined with a single rudder and an actuator disk was modelled in the CFD simulations. The ship geometry is shown in Figure **3**, and its principal characteristics are listed in Table **1**.

Figure 3: The KCS model geometry.

2.3. Simulation Conditions

The migration of the pivot point during the turning circle manoeuvre was analysed through three distinct simulation cases. Table **2** and Figure **4** summarize the simulation cases conducted in this study. Each case is defined by a specific set of environmental parameters: initial wave direction, wavelength, and wave height.

A calm water test was conducted to obtain baseline data under conditions with no external forces applied. To match experimental data, the propeller speed was set at 10.56 RPS, corresponding to a full-scale speed

Table 1: The Main Particulars of the KCS Model used in this Study

Main particulars	Symbols	Full Scale	Model Scale (1:75.24)
Length between the perpendiculars	$L_{BP}(m)$	230	3.057
Length of waterline	$L_{WL}(m)$	232.5	3.0901
Beam at waterline	$B_{WL}(m)$	32.2	0.4280
Draft	D(m)	10.8	0.1435
Displacement	$\Delta(m^3)$	52030	0.1222
Block coefficient	C_B	0.651	0.651
Ship wetted area with rudder	S (m^2)	9530	1.6834
Longitudinal centre of buoyance	$\%L_{BP}$, fwd+	-1.48	-1.48
The metacentric height	GM(m)	0.6	0.008
Radius of gyration	K_{xx}/B	0.4	0.49
Radius of gyration	$K_{yy}/L_{BP}, K_{zz}/L_{BP}$	0.25	0.25
Propeller diameter	$D_P(m)$	7.9	0.105
Propeller rotation direction (view from stern)		Right hand side	Right hand side
Rudder turn rate	(deg./s)	2.32	20.1

Table 2: The Simulation Cases to which the CFD Model is Applied

Case no. C	Approach speed U (m/s)	Propeller rev. (RPM)	Wave height H (m)	Encounter Angle μ (degrees)	Encounter Freq. ω_e (rad/s)	Encounter Period T_e (s)	Wave/ship length λ/L_{BP}
1							
1.1	7.46	73.0	Calm sea	Calm sea	Calm sea	Calm sea	Calm sea
1.2	7.46	92.5	3.6	180 (Head sea)	0.721	8.71	1.00
1.3	8.24	92.5	3.6	225 (Bow sea)	0.676	9.29	1.00
1.4	9.28	92.5	3.6	270 (Beam sea)	0.518	12.14	1.00
1.5	8.93	92.5	3.6	315 (Quartering sea)	0.344	18.24	1.00
1.6	9.11	92.5	3.6	0 ((Following sea)	0.269	23.37	1.00
2							
2.1	9.49	92.5	Calm sea	Calm sea	Calm sea	Calm sea	Calm sea
2.2	7.84	92.5	3.6	225 (Bow sea)	0.838	7.50	0.70
2.3	8.20	92.5	3.6	225 (Bow sea)	0.676	9.29	1.00
2.4	8.88	92.5	3.6	225 (Bow sea)	0.587	10.71	1.30
2.5	9.11	92.5	3.6	225 (Bow sea)	0.520	12.09	1.60
2.6	9.14	92.5	3.6	225 (Bow sea)	0.455	13.82	2.00
Case no. C	**Approach speed U (m/s)**	**Propeller rev. (RPM)**	**Wave height H (m)**	**Encounter Angle μ (degrees)**	**Encounter Period T_e (s)**	**Wave steepness H/λ**	**Wave/ship length λ/L_{BP}**
3							
3.1	9.49	92.5	Calm sea	Calm sea	Calm sea	Calm sea	Calm sea
3.2	8.71	92.5	2.4	225 (Bow sea)	9.15	0.010	1.00
3.3	8.20	92.5	3.6	225 (Bow sea)	9.29	0.016	1.00
3.4	7.60	92.5	4.8	225 (Bow sea)	9.43	0.021	1.00
3.5	7.03	92.5	6.0	225 (Bow sea)	9.58	0.026	1.00
3.6	6.39	92.5	7.2	225 (Bow sea)	9.74	0.031	1.00

of 73 RPM for achieving 14.5 knots (7.46 m/s) in calm water. The propeller speed was adjusted to 13.38 RPS (92.5 RPM at full-scale) to sustain the target speed in head seas; this setting was applied consistently across all wave scenarios (Case 1). In contrast, for Case 2 and 3, the propeller speed was fixed at 13.38 RPS for both calm water and wave conditions to maintain experimental consistency.

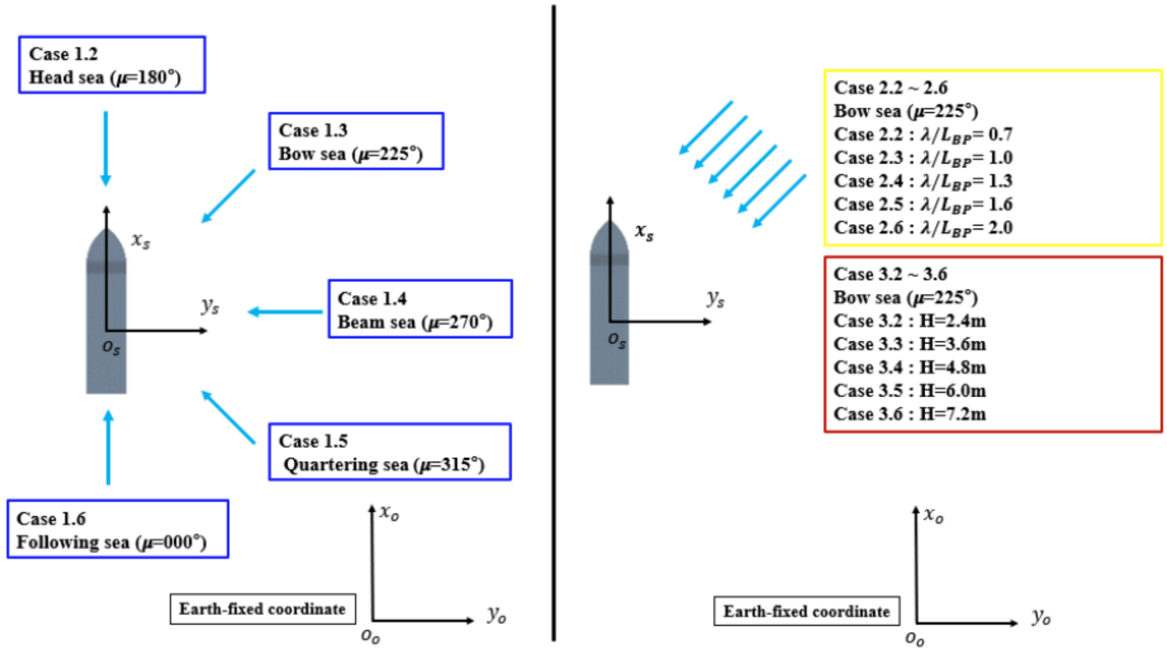

Figure 4: A schematic view of the simulation cases.

In case 1, turning tests were carried out with different wave encounter angle (μ): $180°$, $225°$, $270°$, $315°$ and $0°$. A wave with height $H = 0.048$m in the model scale was selected for the simulation (wave to length ratio $\lambda/L_{BP} = 1.0$ and wave steepness $H/\lambda = 0.016$). These values represented a wave height of 3.6 m in the full-scale.

In case 2, the tests were performed across a range of wavelength to ship length ratios (λ/L_{BP}): 0.7, 1.0, 1.3, 1.6 and 2.0. Since oblique waves generate the strong lateral force and yaw moment, the bow waves ($\mu = 225°$) were chosen in this simulation [3]. Similarly, a wave height was kept consistent with Case 1 at $H = 0.048$ m, which corresponds to a full-scale wave height of 3.6 m.

In case 3, the simulations were conducted with different wave heights (H): 0.032 m, 0.048 m, 0.064 m, 0.080 m and 0.096 m. These wave heights correspond to a range of 2.4 m to 7.2 m in full-scale. The bow waves ($\mu = 225°$) and wavelength to ship length ratio ($\lambda/L_{BP} = 1.0$) were fixed in this simulation.

The encounter frequency of the wave was calculated for every simulation as follows:

$$\omega_e = \omega\left[1 - \frac{\omega U cos\mu}{g}\right] \tag{3}$$

where ω is the wave frequency, U is the ship advance speed, μ is the ship's heading angle relative to the wave direction, and g is the gravitational acceleration.

2.4. Governing Equations

To solve the governing equations, this study employed the Unsteady Reynolds-Averaged Navier-Stokes (URANS) method. For unsteady incompressible flows, the averaged continuity and momentum equations are expressed as below:

$$\frac{\partial(\rho\bar{u}_i)}{\partial x_i} = 0 \tag{4}$$

$$\frac{\partial(\rho\bar{u}_i)}{\partial t} + \frac{\partial}{\partial x_i}\left(\rho\bar{u}_i\bar{u}_j + \rho\overline{u'_i u'_j}\right) = -\frac{\partial\bar{p}}{\partial x_i} + \frac{\partial\bar{\tau}_{ij}}{\partial x_i} \tag{5}$$

In Equitation (5), ρ is the density, $\bar{u}_i$ is the average velocity, x_i represents the Cartesian coordinates, $\rho\overline{u'_i u'_j}$, $\bar{p}$ and $\bar{\tau}_{ij}$ indicate the Reynolds stresses, mean pressure and mean viscous stress tensor, respectively. For a Newtonian fluid, the viscous stress tensor can be expressed as below:

$$\bar{\tau}_{ij} = \mu(\frac{\partial\bar{u}_i}{\partial x_j} + \frac{\partial\bar{u}_j}{\partial x_i}) \tag{6}$$

where μ is the fluid dynamic viscosity. In addition, the RANS method requires a suitable turbulence model to address the Reynolds stresses. A common method employs the Boussinesq theory, expressed as Equitation (7):

$$-\rho\bar{u}_i\bar{u}_j = u_t\left(\frac{\partial\bar{u}_i}{\partial x_j} + \frac{\partial\bar{u}_j}{\partial x_i}\right) - \frac{2}{3}(\rho k + u_t\frac{\partial\bar{u}_k}{\partial x_k})\delta_{ij} \tag{7}$$

where u_t is the eddy viscosity, k is the turbulence kinetic energy and δ_{ij} is the Kronecker delta.

In this simulation, to accurately capture the turbulent flow characteristics around the ship hull, the

Shear Stress Transport (SST) turbulence model was applied for the closure of the governing equations. This model effectively utilizes a blending function to transition from a $k-\omega$ formulation near the wall to a $k-\varepsilon$ formulation in the far-field. Moreover, the fluid flow simulation utilized the Finite Volume Method (FVM), which discretizes the computational domain into adjacent control volumes. This approach converts the governing equations into solvable algebraic equations and is particularly effective for the complex geometries such as a ship hull. Additionally, a predictor-corrector algorithm was utilized for effective pressure-velocity coupling in the URANS solver.

2.5. Coordinate System

Figure **5** illustrates all coordinate systems used in this simulation. Four coordinate systems were applied to analyse dynamic kinematic data based on turning manoeuvre simulations, as described below:

(1) Earth-fixed coordinate system $(O_O - x_O y_O z_O)$

(2) Ship-fixed coordinate system $(O_S - x_S y_S z_S)$

(3) Propeller-fixed coordinate system $(O_p - x_p y_p z_p)$

(4) Rudder-fixed coordinate system $(O_r - x_r y_r z_r)$

The Earth-fixed coordinate system serves as an absolute reference frame. As an inertial system fixed to a specific point, it allows neither translation nor rotation. In contrast, the ship-fixed coordinate system was fixed to the vessel's centre of mass and moved in tandem with the ship's motion. Within this coordinate system, the 6-DOF equations of motion were formulated and solved. The propeller-fixed and rudder-fixed coordinate systems were implemented for the positioning of the actuator disk and the control of the rudder angle, respectively. Regarding the rudder-fixed coordinate system, the rudder blade rotates about the Z_r axis, which represents the rudder stock axis.

2.6. Mesh Generation and Boundary Condition

The numerical grid was generated using the automatic meshing facility in STAR-CCM+, which produces high-fidelity surface and volume meshes. To accurately represent the complex geometry of the ship hull, a surface remesher was utilized, while the Prism Layer mesh model was applied to precisely resolve the near-wall boundary layer flow. For the volume mesh, a trimmed cell mesher was adopted to create an unstructured hexahedral grid system. Furthermore, additional mesh refinements were implemented in localized regions, such as the bow, stern, and rudder gap. These enables a more accurate and reliable analysis of areas with steep flow gradients. Following ITTC guidelines, the free surface was also refined to ensure sufficient resolution for capturing wave characteristics [20]. By employing these meshing features, the total cell count was optimized to 6.90 million for calm water (Cases 1.1, 2.1, and 3.1) and 7.19 million for wave conditions (other cases), ensuring high-fidelity analysis even under complex flow environments. Grid structure of domain in this paper are shown in Figure **6**.

The computational domain was divided into background, hull, and rudder regions. These regions were integrated using the overset grid technique to allow for independent motion between the bodies, which is essential for simulating complex ship manoeuvre [21].

Specific boundary conditions were assigned to each section of the computational domain to represent the physical environment. A pressure outlet was assigned to the top of the domain to represent the atmosphere [5]. The inlet, outlet, side, and bottom boundaries were set as velocity inlet to ensure steady flow characteristic of an open water environment while preventing non-physical disturbances [22]. Furthermore, non-slip wall conditions were used for moving surfaces such as the ship hull and rudder [23].

Numerical stability was further ensured by employing the damping method for calm water simulations to prevent wave reflections. For wave simulations, however, the forcing method was applied to maintain incident wave conditions and effectively eliminate ship-induced disturbances.

2.7. Turning Module

To analyse the dynamic movement of the pivot point under wave conditions, a turning circle manoeuvre was performed with a 35° starboard rudder angle. To ensure precise initial conditions prior to the manoeuvre, the ship's state was monitored to confirm a constant approach speed and a steady course. This stabilization was achieved by maintaining a fixed propeller RPM and employing a Proportional-Integral-Derivative (PID) controller, commonly used in industrial control systems, to regulate rudder angle. The rudder angle was regulated by a PID feedback controller, which commands port or starboard movements. The function of this control law is given by:"

$$\delta(t) = K_p e(t) + K_i \int_0^t e(t)dt + K_d \frac{de(t)}{dt} \tag{8}$$

$$e(t) = \psi(t) - \psi_c \tag{9}$$

where $\delta(t)$ is the rudder angle, $\psi(t)$ is the current yaw angle, ψ_c is the target yaw angle which must be set to 0 to maintain ship's heading. K_p, K_i, and K_d

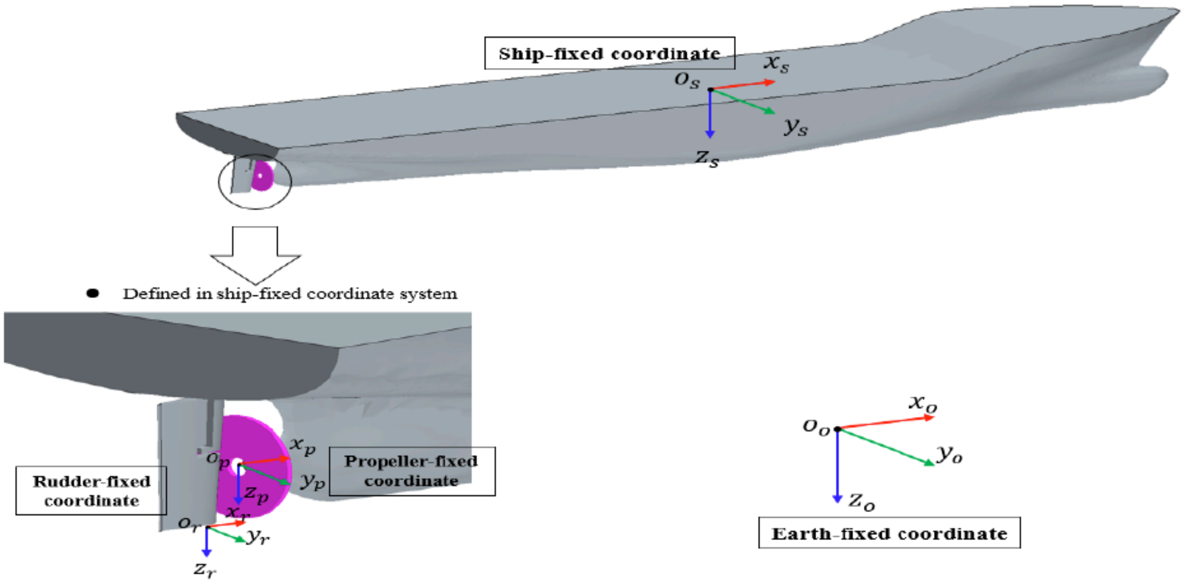

Figure 5: The coordinate system of the simulation cases.

means the proportional, integral, and derivative control gains, respectively. Appropriate gain values must be selected to achieve optimal regulation of the rudder angle. In this paper, these values were chosen as $K_p = 5, K_i = 0.05, and\ K_d = 3$ and the same gain values were applied for all other wave conditions.

In every simulation, a 35° starboard turning circle test was conducted. The rudder angle $\delta(t)$ was determined using the following equations:

$$\delta(t) = \begin{cases} \max(0, kt), \delta \leq 35 \\ 35 \end{cases} \quad (5)$$

where k is the maximum rudder rate. In this study, the maximum rudder rate was $k = 20.1\ deg/s$, which corresponds to $2.32\ deg/s$ in full scale and the rudder angle was maintained at 35 degrees throughout the turning circle test.

3. RESULTS AND DISCUSSION

In this study, numerical simulations based on Computational Fluid Dynamics (CFD) were performed by setting the primary wave parameters (initial direction, length and height) as variables. All parameters and numerical results are presented in full-scale values, although the simulations were conducted at model scale. Each scenario aimed to derive the time-series response of the longitudinal shift of the pivot point resulting from a turning manoeuvre with a maximum starboard rudder angle. Data analysis covered a complete 360-degree turn starting from the initial heading. In this process, the rapid divergence of GP value immediately after rudder execution is due to the vessel entering a complex coupled motion of sway and yaw, driven by simultaneous yaw moments and lateral forces [13]. In the following analysis and figures, several black dashed lines indicate the points where the ship's heading changes by every 45-degree increment. To provide a generalized analysis, GP value was non-dimensionalised by the ship's length(L_{BP}) as follows:

$$GP' = \frac{GP}{L_{BP}}$$

In the following sections, GP denotes the non-dimensionalised value unless otherwise stated.

3.1. Validation Study

The CFD analysis methodology adopted in this study is a model whose accuracy and reliability have already been sufficiently validated for free-running and wave-induced manoeuvring simulations.

In the author's previous study using the same numerical methodology, the simulated results were found to be in good agreement with the experimental data [3]. In that prior study, grid and time step sensitivity analyses were carried out, and the numerical uncertainty evaluated via the GCI (Grid Convergence Index) method was no greater than 0.28% in space and 0.19% in time, demonstrating a high level of numerical accuracy. Furthermore, as shown in Tables **3** and **4**, the simulated turning trajectories and key manoeuvring parameters in both calm water and waves showed reasonable agreement with the model test results conducted at Hiroshima University [24]. These parameters are the direct kinematic consequences of the sway velocity(v) and yaw rate(r) derived in the present study.

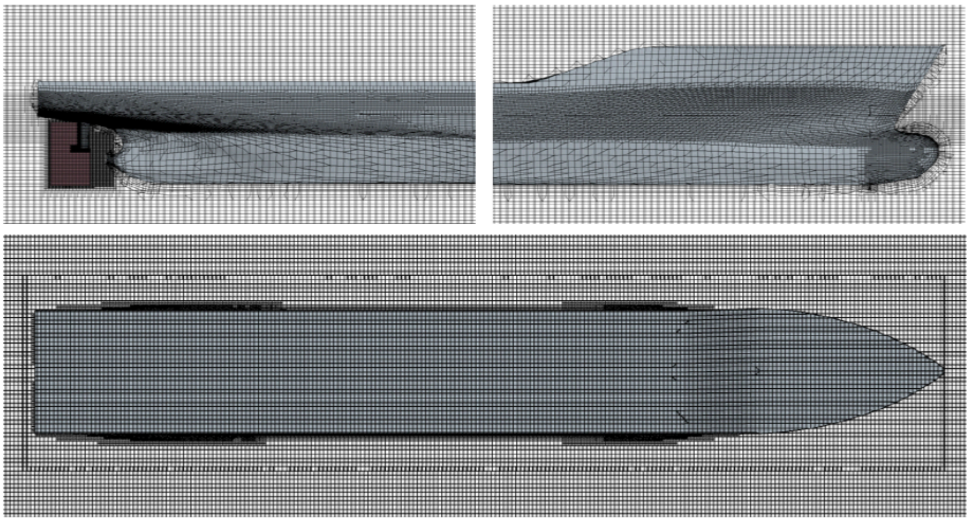

(**a**) Surface mesh

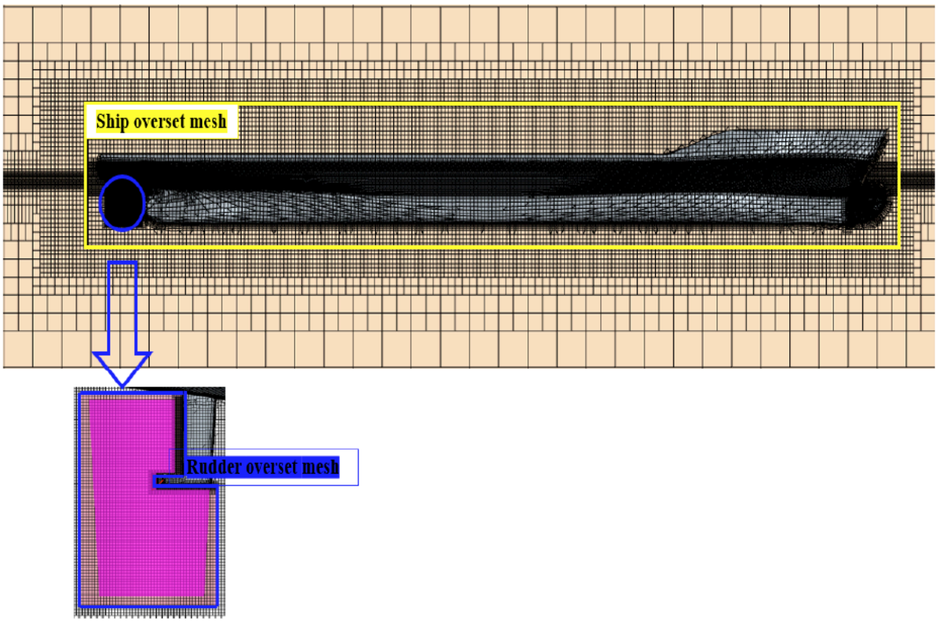

(**b**) Volume mesh

Figure 6: Computational mesh: **a**) Surface mesh **b**) volume mesh.

Consequently, the simulations in this study were performed using the validated grid and time-step settings established in the prior work, without additional verification. The dynamic pivot point analysis based on the manoeuvring response data obtained from these simulations is therefore considered to have sufficient engineering validity and reliability.

Table 3: Comparison of Manoeuvring Parameters in Calm Sea

Parameters (Calm sea)	Result		Error (%)
	CFD	EFD	
Advance (m)	9.30	9.29	0.01
Transfer (m)	3.95	4.16	-4.86
Tactical diameter (m)	9.94	9.66	2.89

Table 4: Comparison of manoeuvring parameters in head sea

Parameters (Head sea)	Result		Error (%)
	CFD	EFD	
Advance (m)	7.86	8.20	-4.11
Transfer (m)	3.09	3.35	-7.78
Tactical diameter (m)	7.97	8.37	-4.83

3.2. GP Response Analysis for Different Initial Wave Directions

In this section, the dynamic movement characteristics of the pivot point during ship turning were analysed with the Initial Wave Encounter Angle as a variable. The time-series response results of GP value for each condition are presented in a total of 6 figures, from Figure **7**(**a**) to Figure **7**(**f**). Detailed comparison data can be found in Table **5**. Furthermore, to ensure a more stable and analytical comparison, the mean GP values were calculated for the period from 50 seconds after the rudder execution until the end of the manoeuvre. In terms of the wave encounter angles, GP response did not depend solely on the initial wave direction; instead, it exhibited complex patterns of change according to the shifting wave encounter angles during the turning process. The most significant GP fluctuations occurred when the wave encounter angle was between the beam and the stern.

Figure **7**(**a**) illustrates that GP fluctuations were minimal under the calm water condition, forming a smooth baseline consistent with the turning manoeuvre. As the turn progressed, the pivot point shifted gradually forward, reaching the forward end of the ship (approximately $GP' = 0.5$) by the time the heading had changed by 90°. As the manoeuvre continued, GP value gradually decreased, with the pivot point eventually stabilizing at approximately 0.1L from the bow toward the centre of gravity. These results serve as a significant control group for quantifying the net impact of external wave forces on GP data.

Under the head sea (μ = 180°) condition, as shown in Figure **7**(**b**), the initial GP variation remained relatively stable due to symmetric wave loads acting on the hull. However, as the encounter angle transitioned from bow to beam sea, the GP amplitude progressively amplified to a peak of 0.86, driven by the low initial yaw rate that reflects the vessel's directional inertia in head sea.Additionally, the gap between the converged locations of the pivot point at the start and the end of the turn reached its maximum. As the turning manoeuvre progressed, the pivot point shifted continuously forward, eventually moving beyond the ship's bow around 140 seconds into the simulation.

In Figure **7**(**c**), under the bow sea (μ = 225°) condition, the initial overshoot was the most significant among all simulations. This is attributed to the relatively large fluctuations in yaw velocity and moment typically observed in oblique waves. High-amplitude oscillations emerged immediately after the onset of the manoeuvre; however, these gradually stabilized as the ship turned and the encounter angle shifted toward the head sea condition. Furthermore, the turning manoeuvre initiated from the bow sea converged a relatively high yaw rate (r) throughout the process. This sustained rotational momentum, combined with the transition to head waves, effectively suppressed the initial variability, leading GP value to converge toward a stable result of 0.46. Consequently, the pivot point was found to be well-contained within the ship's length, ensuring that the turning centre was established at a predictable location inside the hull.

As shown in Figure **7**(**d**), GP value exhibited highly abrupt fluctuations immediately upon the initiation of the turning manoeuvre under the beam sea (μ = 270°) condition. This is primarily due to the fact that the largest fluctuations in sway velocity and forces occur when the vessel is subjected to beam wave. However, as the manoeuvre progressed and the encounter angle transitioned toward the longitudinal wave region, the amplitude stabilized or slightly attenuated following the initial excitation.

As shown in Figure **7**(**e**), the quartering sea (μ = 315°) condition commenced with a relatively consistent level of oscillation. Notably, in contrast to the bow sea, the following sea exhibited significantly lower instability during the initial phase of rudder angle increase. This suggests that waves approaching from the stern impose a comparatively smaller initial excitation on GP value. However, transitioning toward a 270° encounter angle intensified GP amplitudes due to beam sea interference. As the ship further turned into the head and bow sea sectors, these forward-incident waves effectively dampened the oscillation amplitude. Nevertheless, this transition simultaneously hindered the yaw rate through increased rotational resistance, driving the GP momentarily beyond the bow. Once the vessel passed the head sea sector, the reduced wave drag restored the yaw rate, allowing the GP to revert to its stable position within the hull boundary.

Finally, as shown in Figure **7**(**f**), the following sea ($\mu = 000°$) condition exhibited a high level of initial stability at the onset of the turn. Aside from minor fluctuations during the initial rudder execution, GP value increased steadily without any sharp peaks, demonstrating the stability of GP behaviour in following sea. GP value increased gradually during the turn but eventually shifted outside of the ship’s length upon entering the bow and head sea sectors. The pivot point remained outside the hull while passing through the head sea region. It returned to and stabilized within the hull boundary only after the vessel moved beyond these forward-incident waves

Conclusively, the following sea condition exhibited a high level of initial stability, whereas the bow sea induced the most pronounced initial overshoot. Across all simulations, the transition between oblique and beam sea emerged as the most critical phase, where peak oscillations and uncertainty were maximized. This is attributed to the fact that sway velocity fluctuations are most severe in beam sea, while yaw velocity oscillations peak in oblique waves, particularly in quartering sea [3, 4]. Furthermore, in cases starting from longitudinal waves, such as head and following sea, significant longitudinal migrations of the pivot point were observed due to their convergence toward relatively lower yaw rates. Notably, in the head sea scenario, the pivot point remained consistently beyond the bow after 140 seconds due to a precipitous drop in the yaw rate. In contrast, for beam and oblique sea conditions, the pivot point remained within the hull boundary throughout most of the manoeuvre, supported by their relatively higher convergence yaw rates.

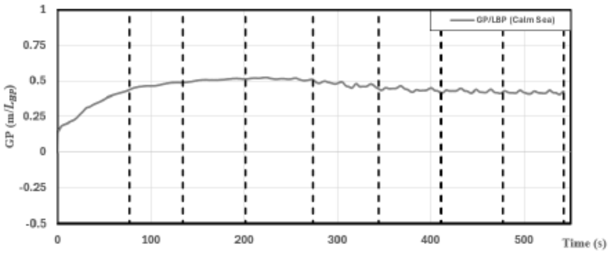

(**a**) Calm sea

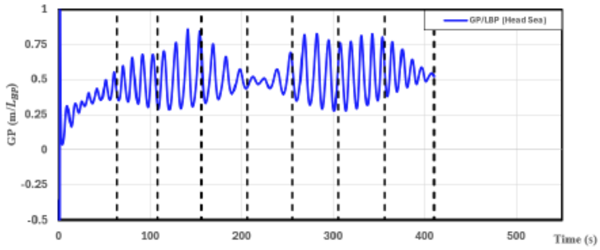

(**b**) Head sea ($\mu = 180°$)

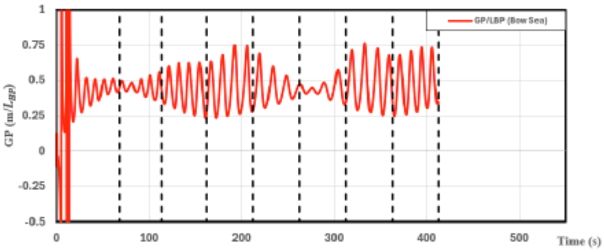

(**c**) Bow sea ($\mu = 225°$)

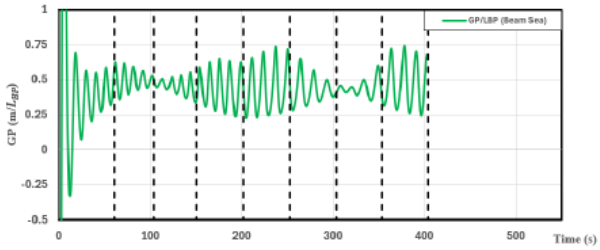

(**d**) Beam sea ($\mu = 270°$)

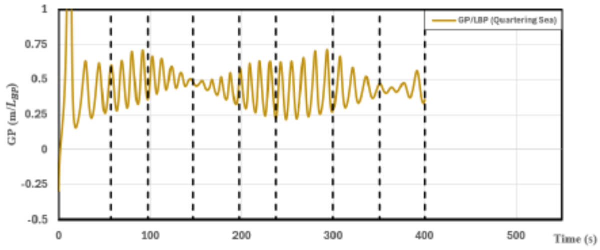

(**e**) Quartering sea ($\mu = 315°$)

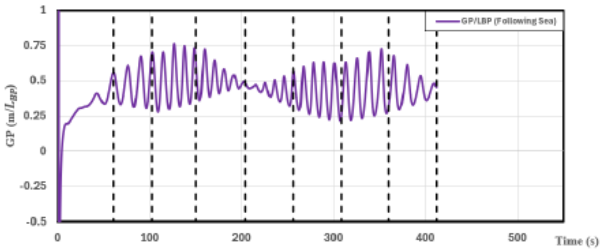

(**f**) Following sea ($\mu = 0°$)

Figure 7: Time-series GP responses for different initial wave directions.

Table 5: Summary of Peak and Mean GP Values for Different Initial Wave Directions

Case 1	Peak GP		Mean GP
	Value	Time(s)	Value
1.1 (Calm sea)	0.52	223	0.43
1.2 (Head sea)	0.86	141	0.51
1.3 (Bow sea)	0.76	323	0.46
1.4 (Beam sea)	0.74	378	0.45
1.5 (Quartering sea)	0.71	293	0.44
1.6 (Following sea)	0.76	126	0.45

3.3. GP Response Analysis for Different Wavelengths

Figure **8** and Table **6** illustrate the non-dimensionalised time-series response of GP and a summary of GP values during a standard turning manoeuvre under various wavelength conditions. The wavelength to ship length ratio (λ/L_{BP}) ranged from 0.7 to 2.0. In this simulation, bow sea ($\mu = 225°$**)** was specifically focused on, as oblique sea conditions induce significant lateral forces and yaw moments that critically affect the vessel's trajectory [3-5].

Figure **8**(**a**) illustrates the GP response characteristics during the turning manoeuvre under calm water condition. To ensure a consistent comparison with the wave conditions, the propeller speed was set at 92.5 RPM. The experimental results show that as the turn progressed, GP value increased gradually and tended to converge to approximately 0.45. These calm water results serve as a critical control group for quantifying the net impact of external wave forces on the GP data.

In general, the variation of GP was most pronounced in Case 2.2 (λ/L_{BP} =1.0). This is resulted from the fact that the encounter frequency in the bow sea condition (λ/L_{BP}=1.0, T_e= 0.93Hz) approximated the natural frequency of the vessel, inducing resonant oscillations. Accordingly, the fluctuation of GP decreased as the wavelength ratio deviated from 1.0. Compared to the peak observed at λ/L_{BP} = 1.0, the maximum GP value was reduced to 80%, 75%, and 70% at λ/L_{BP} values of 1.3, 1.6, and 2.0, respectively. This phenomenon is attributed to reduced wave steepness from longer wavelengths at constant wave height and an increased yaw rate, which collectively stabilize the GP response [4].

Notably, when waves were encountered from the stern, GP fluctuations were significantly more pronounced at λ/L_{BP} = 0.7 than at 1.0. This is because the wave of λ/L_{BP} = 0.7, with its slower phase velocity, stays in contact with the hull's slope for a longer duration, thereby prolonging the state of compromised stability. As illustrated in Figure **8**(**b**), GP value initially converged to an average of 0.4 after the turn stabilized. However, as the vessel passed through following sea and reached quartering sea conditions, GP fluctuations spiked abruptly, with exceeding 0.5. This indicates that the pivot point shifted beyond the vessel's hull boundary, signalling a critical loss of directional stability.

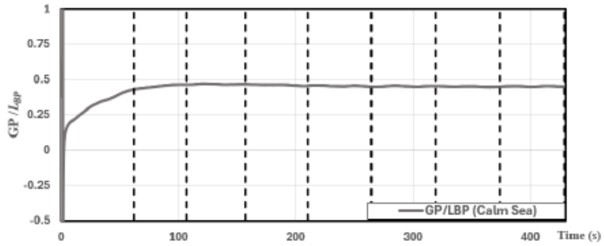

(**a**) Calm Sea

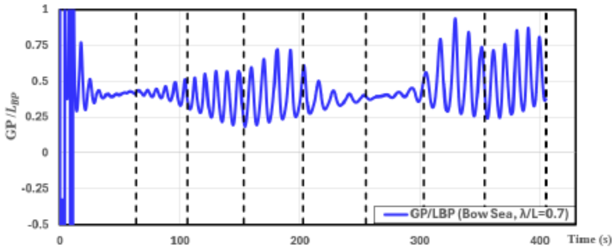

(**b**) Bow sea (λ/L_{BP}=0.7)

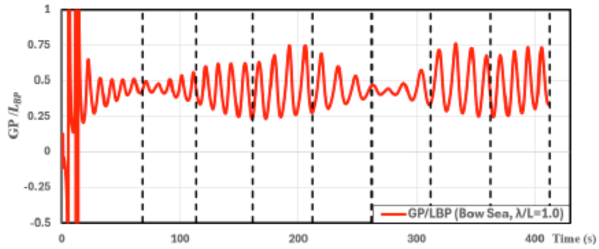

(**c**) Bow sea (λ/L_{BP}=1.0)

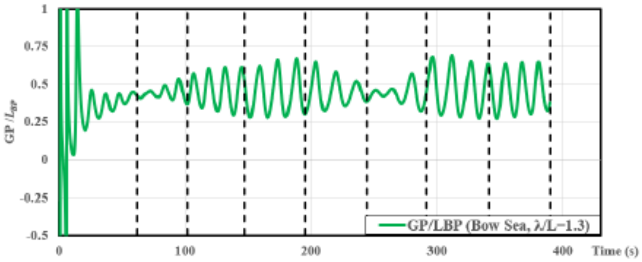

(**d**) Bow sea (λ/L_{BP}=1.3)

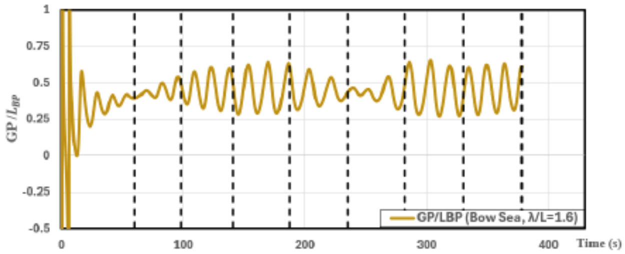

(**e**) Bow sea (λ/L_{BP}=1.6)

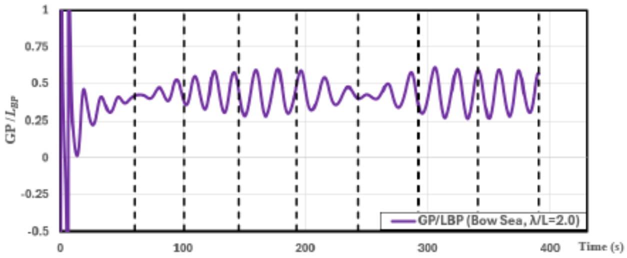

(**f**) Bow sea (λ/L_{BP}=2.0)

Figure 8: Time-series GP responses for different wavelengths.

Table 6: Summary of Peak and Mean GP Values for Different Wavelengths

Case 2	Peak GP		Mean GP
	Value	Time(s)	Value
2.1 (Calm sea)	0.47	121	0.45
2.2 (λ/L_{BP}=0.7)	0.94	329	0.43
2.3 (λ/L_{BP}=1.0)	0.76	323	0.45
2.4 (λ/L_{BP}=1.3)	0.69	311	0.45
2.5 (λ/L_{BP}=1.6)	0.65	302	0.44
2.6 (λ/L_{BP}=2.0)	0.61	305	0.43

3.4. GP Response Analysis for Different Wave Heights

Figure **9** and Table **7** illustrate the non-dimensionalised time-series response of GP and its associated values during a standard turning manoeuvre across various wave heights, ranging from 2.4m to 7.2m in full-scale. For this simulation, bow wave ($\mu = 225°$) was specifically applied, and the propeller speed was maintained at a constant 92.5 RPM for all cases. Figure **9**(**a**) illustrates GP response baseline during turning circle manoeuvre under calm water condition.

Under consistent conditions, the converged yaw rate decreased as wave height increases. However, GP value is not determined solely by the yaw rate; thus, it did not maintain a simple linear relationship with wave height. As illustrated in Figures **9**(**a**) through (**f**), higher wave heights significantly amplified the fluctuations of GP. This non-linear escalation was attributed to both the increased instability of the data and the markedly reduced yaw rate caused by heightened wave resistance.

In Figure **9**(**b**) and (**c**), under wave heights of H =2.4m and H =3.6m, GP value converged to approximately 0.45 throughout the turning manoeuvre, showing no significant deviation from calm water conditions. In contrast, for wave heights of H=4.8m and H=6.0m, the peak GP value exceeded 1.0 and 1.8, respectively as seen in Figures **9**(**d**) and (**e**). This implies that the pivot point fluctuated forward by two to three times the distance from the centre of gravity to the bow.

Regarding the longitudinal position of the pivot point under these conditions (H= 4.8 m and 6.0 m), GP value rose with unstable oscillations during the initial phase until the ship encountered head wave. Subsequently, it tended to decrease temporarily after passing the head-wave zone, corresponding to the stage where the yaw rate began to recover incrementally. However, as the ship passed the following sea and entered the starboard quartering sea phase, GP fluctuations reached their maximum, and the values surged abruptly. In this region, where the vessel reached the latter half of the turn, the averaged value of GP increased by approximately 15% at H=4.8 m and 30% at H=6.0 m compared to calm water conditions. This significant surge was primarily driven by the rapid escalation in sway velocity within the quartering sea phase.

In Figure **9**(**f**), GP fluctuations became severe, reaching a peak of approximately 28.0 in the quartering sea zone, representing a highly unstable state in the highest wave (H =7.2m). This extreme peak was attributed to the momentary reduction of the yaw rate near zero.

In conclusion, increased wave height exerted a decisive influence on GP variability and accelerated the longitudinal shift of the pivot point during manoeuvre. The forward shift of the pivot point in the early stages was caused by the reduction in yaw moment due to wave resistance. In contrast, the significant GP increase in the mid-to-late stages was dominated by a rapid rise in sway velocity rather than yaw rate effects.

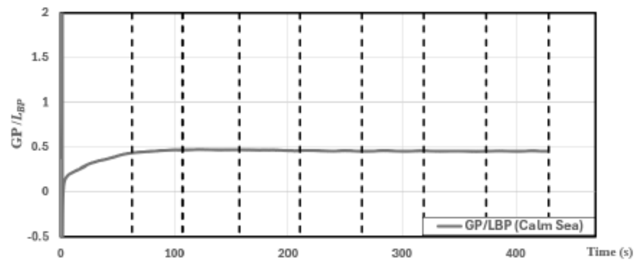

(**a**) Calm sea

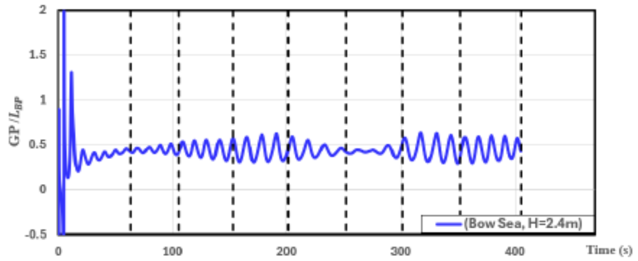

(**b**) Bow sea (H=2.4m)

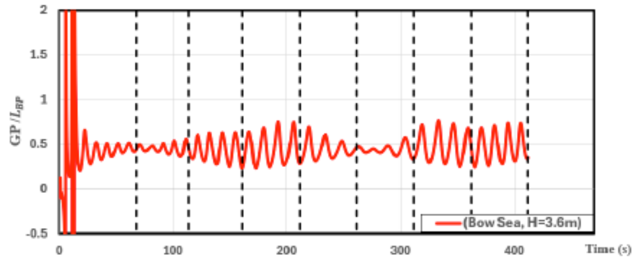

(**c**) Bow sea (H=3.6m)

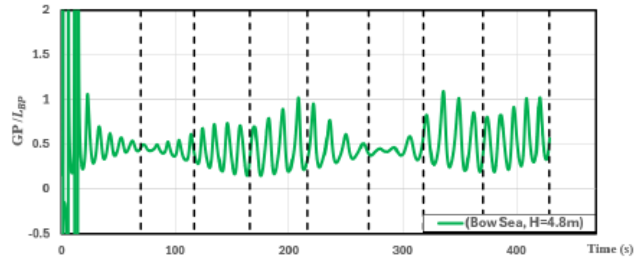

(**d**) Bow sea (H=4.8m)

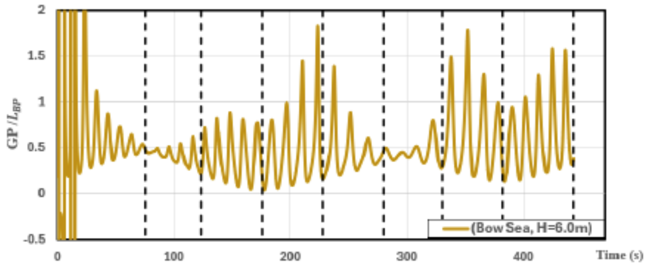

(**e**) Bow sea (H=6.0m)

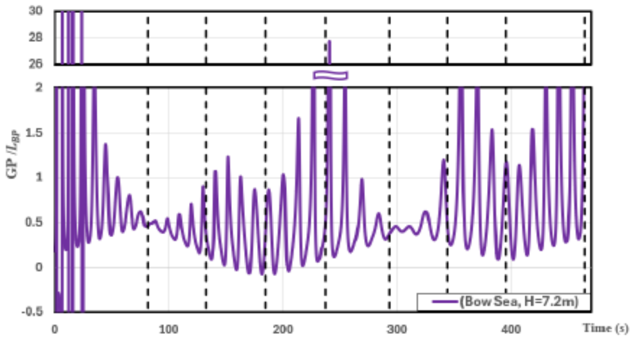

(**f**) Bow sea (H=7.2m)

Figure 9: Time-series GP responses for different wave heights.

Table 7: Summary of Peak and Mean GP values for Different Wave Heights

Case 3	Peak GP		Mean GP
	Value	Time(s)	Value
3.1 (Calm sea)	0.47	121	0.45
3.2 (H=2.4m)	0.63	318	0.44
3.3 (H=3.6m)	0.76	323	0.45
3.4 (H=4.8m)	1.09	336	0.47
3.5 (H=6.0m)	1.83	223	0.51
3.6 (H=7.2m)	27.7	240	0.66

4. CONCLUDING REMARKS

4.1. Conclusions

This study systematically investigated the dynamic migration of the pivot point for the KCS vessel across a wide range of wave conditions. By incorporating variables such as initial direction, wavelength, and wave height, this work addressed key phenomenon often overlooked in conventional manoeuvring research. By analysing the correlation between pivot point shifts and wave parameters, this research clarified how real sea states influence ship manoeuvrability. The key findings are summarized as follows:

1) In the investigation of initial wave directions, it was found that the stability of the initial pivot point was high when turning commenced under head/following sea conditions, whereas the greatest fluctuation of the pivot point was observed under oblique sea conditions, particularly in bow sea (μ = 315°). Notably, as a turn initiated in head sea transitions into the stern-quartering phase, the pivot point advanced sharply beyond the bow. This implies that wave impact on the stern, combined with a diminished yaw rate, triggers the sharp advancement of the pivot point. Consequently, while initial turning in oblique and beam sea exhibits high instability, turns initiated in head sea require careful attention to changes in manoeuvring characteristics caused by the sharp forward migration of pivot point as the ship moves into the following-to-quartering wave section.

2) In the investigation of manoeuvring characteristics across various wavelength conditions, the fluctuations of GP were most pronounced when the wavelength-to-ship length ratio (λ/L_{BP}) was 1.0. This was attributed to the resonance phenomenon, triggered when the wave encounter frequency approximated the vessel's natural frequency. Conversely, as the wavelength ratio increased beyond 1.0, GP variation showed a stabilizing trend. Compared to the peak observed at $\lambda/\mathrm{L_{BP}}$=1.0, the maximum GP values were reduced to 80%, 75%, and 70% at $\lambda/\mathrm{L_{BP}}$ values of 1.3, 1.6, and 2.0, respectively. This stabilization occurred because, under constant wave height, an increase in wavelength reduces wave steepness and promotes a higher yaw rate. Notably, however, under the shortest wave condition ($\lambda/\mathrm{L_{BP}}$=0.7), GP fluctuations while encountering waves from the stern were found to be even more significant than those observed at the resonance condition ($\lambda/\mathrm{L_{BP}}$=1.0). This is due to the lower phase velocity of short wave, which leads to a prolonged residence time on the wave crest or slope. While GP value typically converged to approximately 0.05~0.1L from the bow under other wavelength conditions, it was observed to advance sharply and migrate beyond the bow when encountering waves from the stern at shortest wave ($\lambda/\mathrm{L_{BP}}$=0.7). In conclusion, while resonance should be a primary concern when encountering waves from the bow at $\lambda/\mathrm{L_{BP}}$=1.0, particular attention must be paid to the abrupt forward migration of the pivot point caused by short waves during the subsequent stern-quartering phase.

3) For the analysis of the impact of wave height on the dynamic migration of pivot point, its variability exhibited nonlinear amplification that accelerated rapidly with increasing wave height. At lower wave heights (H=2.4m and H=3.6m), GP value converged stably near 0.45, consistent with calm water behaviour; however, once wave height exceeds H=4.8m, dynamic instability intensified sharply, with peak GP value surpassing 1.0. At the maximum wave height of H=7.2m, GP peak value reached approximately 28, representing an extreme condition in which the pivot point migrated well beyond the forward boundary of the

hull. This behaviour was attributed to the increasingly extreme manifestations of the physical factors governing GP at each stage of the turn as wave height increases. During the initial turning phase, when the vessel encountered waves from the bow, the rate of yaw decreased more sharply with increasing wave height, acting as the primary driver of forward migration of the pivot point. As the turn progressed into the mid-to-late phase and the vessel transitioned into the quartering sea from the following sea, the governing mechanism shifted from yaw rate reduction to a rapid increase in sway velocity. The magnitude of this sway velocity increase grew proportionally with wave height, and under severe wave conditions, the resulting disruption of force equilibrium displaced the pivot point beyond the hull boundary, posing a critical risk of loss of directional control. These findings underscore that manoeuvring in heavy weather demands heightened caution, with particular attention to the abrupt changes in manoeuvring response.

This work systematically characterized the dynamic shift behaviour of the pivot point in waves by analysing its migration across varying initial wave directions, wavelengths, and wave heights. The results demonstrate that the pivot point is dynamically repositioned by changes in hydrodynamic moments driven by sway and yaw motions. This finding goes beyond the simplified assumptions of conventional studies, offering a more physics-based understanding of pivot point behaviour.

These studies carry practical implications beyond their academic value. The pivot point migration trends identified in this study can serve as a practical reference for operators. This enables them to anticipate changes in rudder effectiveness and turning moment when manoeuvring under adverse and complex wave conditions. From a mechanical engineering perspective, anticipating pivot point shifts helps prevent control response degradation. By preventing excessive rudder commands triggered by the operator's perceived instability, it is possible to minimize momentary peak loads and mechanical fatigue on the steering machinery. This ensures the vessel’s dynamic interactions remain within safe mechanical limits, enhancing operational reliability in stochastic environments.

4.2. Limitations and Future Works

Despite these academic and practical contributions, the present study has several limitations. First, the target hull form is limited to a single hull, the KCS. This constrains the generalizability of the movement characteristics of the pivot point to various hull forms. Furthermore, the simulations were conducted exclusively under a specific propeller speed condition. This is insufficient to fully capture the dynamic response characteristics of the pivot point across varying operational speeds.

Therefore, future research should expand the scope of analysis to diverse hull forms, such as tankers and passenger vessels with complex superstructures. This expansion will help further analyse how different hull forms influence pivot point behaviour and reveal the underlying relationships between hull form characteristics and pivot point movement. Further investigation into the pivot point movement characteristics under low-speed manoeuvring conditions is needed. Such conditions include berthing and unberthing situations that are critically important in actual port operations. These efforts are planned with the aim of improving the accuracy of harbour manoeuvring performance prediction and ensuring maritime traffic safety.

ACKNOWLEDGEMENTS

This research was supported by the Ministry of SMEs and Startups(MSS), Korea Institute for Advancement of Technology(KIAT) through the Innovation Development(R&D) for Global Regulation-Free Special Zone.

REFERENCES

[1] Allianz Global Corporate & Specialty. Safety and shipping review 2018. Munich: Allianz; 2018 https://commercial.allianz.com/news-and-insights/news/safety-shipping-review-2018.html

[2] International Maritime Organization. Symposium on "making headway on the IMO MASS Code” London: IMO; 2023 May https://www.imo.org/en/mediacentre/meetingsummaries/pages/symposium-on-%CA%BAmaking-headway-on-the-imo-mass-code%E2%80%9D-.aspx

[3] Kim D, Song S, Tezdogan T. Free running CFD simulations to investigate ship manoeuvrability in waves. Ocean Eng 2021; 236: 109567. https://doi.org/10.1016/j.oceaneng.2021.109567

[4] Kim D, Song S, Jeong B, *et al*. Numerical evaluation of a ship's manoeuvrability and course keeping control under various wave conditions using CFD. Ocean Eng 2021; 237: 109615. https://doi.org/10.1016/j.oceaneng.2021.109615

[5] Kim D, Song S, Jeong B, *et al*. Unsteady RANS CFD simulations of ship manoeuvrability and course keeping control under various wave height conditions. Appl Ocean Res 2021; 117: 102940. https://doi.org/10.1016/j.apor.2021.102940

[6] Kim D, Tezdogan T. CFD-based hydrodynamic analyses of ship course keeping control and turning performance in irregular waves. Ocean Eng 2022; 248: 110808. https://doi.org/10.1016/j.oceaneng.2022.110808

[7] Kim D, Tezdogan T, Incecik A. Hydrodynamic analysis of ship manoeuvrability in shallow water using high-fidelity URANS computations. Appl Ocean Res 2022; 123: 103176. https://doi.org/10.1016/j.apor.2022.103176

[8] Rowe RW. The shiphandler's guide for masters and navigating officers, pilots and tug masters. 2nd ed. London: Nautical Institute; 2000.

[9] ITTC. Tasks and structure of the 29th ITTC technical committees and groups. Proceedings of the 29th International Towing Tank Conference; 2021.

[10] International Conference on Marine Simulation and Ship Manoeuvrability. Marsim 2015; 2015 Sep 8-11; Newcastle upon Tyne, UK.

[11] Seo SG, Mishu M. The use of pivot point in ship handling for safer and more accurate ship manoeuvring. Proceedings of IMLA. 2011 Oct 1; 1(29): 271-80. https://www.academia.edu/36456506/The_Use_of_Pivot_Point_in_Ship_Handling_for_Safer_and_More_Accurate_Ship_Manoeuvring.

[12] Seo SG. Safer and more efficient ship handling with the pivot point concept. The International Journal on Marine Navigation and Safety of Sea Transportation.2016; 10(4): 605-12. https://doi.org/10.12716/1001.10.04.09

[13] Serhii Z, Oleh T. What is the Pivot Point and how to use it to control the vessel. In: Materials of the XII International Scientific and Practical Conference "Advanced Information and Innovative Technologies for Transport (MINTT–2020)"; 2020.

[14] Serhii Z, Oleh T, Pavlo N, *et al.* Pivot point position determination and its use for manoeuvring a vessel. Ships Offshore Structures 2023; 18: 358-64. https://doi.org/10.1080/17445302.2022.2052480

[15] Mofidi A, Carrica PM. Simulations of zigzag maneuvers for a container ship with direct moving rudder and propeller. Comput Fluids 2014; 96: 191-203. https://doi.org/10.1016/j.compfluid.2014.03.017

[16] Shen Z, Wan D, Carrica PM. Dynamic overset grids in OpenFOAM with application to KCS self-propulsion and maneuvering. Ocean Eng 2015; 108. https://doi.org/10.1016/j.oceaneng.2015.07.035

[17] Wang J, Zou L, Wan D. CFD simulations of free running ship under course keeping control. Ocean Eng 2017; 141: 450-64. https://doi.org/10.1016/j.oceaneng.2017.06.052

[18] Wang J, Zou L, Wan D. Numerical simulations of zigzag maneuver of free running ship in waves by RANS-Overset grid method. Ocean Eng 2018; 162: 55-79. https://doi.org/10.1016/j.oceaneng.2018.05.021

[19] Inoue K. Theory and practice of ship handling. Tokyo: Seizando; 2000.

[20] ITTC. Practical guidelines for ship CFD applications. Proceedings of the 26th International Towing Tank Conference; 2011.

[21] Koomullil R, Soni B, Singh R. A comprehensive generalized mesh system for CFD applications. Math Comput Simul 2008; 78: 605-17. https://doi.org/10.1016/j.matcom.2008.04.005

[22] Kim D, Jeong B. Investigation on toxicity of ammonia releasing from storage tank onboard through CFD simulations. J Int Marit Saf Environ Aff Shipp 2024; 8: 2339342. https://doi.org/10.1080/25725084.2024.2339342

[23] Scotto di Perta E, Agizza MA, Sorrentino G, *et al.* Study of aerodynamic performances of different wind tunnel configurations and air inlet velocities, using computational fluid dynamics (CFD). Comput Electron Agric 2016; 125: 137-48. https://doi.org/10.1016/j.compag.2016.05.007

[24] Yasukawa H, Hasnan MAA, Matsuda A. Validation of 6-DOF motion simulations for ship turning in regular waves. J Mar Sci Technol. 2021; 26: 1096-1111. https://doi.org/10.1007/s00773-020-00793-8

---

https://doi.org/10.31875/2409-9848.2026.13.03